Vibrational spectral investigation and natural bond orbital analysis of pharmaceutical compound 7-Amino-2,4-dimethylquinolinium formate – DFT approach

D.M. Suresh [a], M. Amalanathan [b,*], S. Sebastian [c], D. Sajan [d], I. Hubert Joe [e], V. Bena Jothy [f], Ivan Nemec [g]

[a] Department of Physics, Government Arts College, Udhagamandalam, Tamil Nadu, India
[b] Annai Velankanni College, Department of Physics, Tholayavattam 629 157, Tamil Nadu, India
[c] Department of Physics (Science and Humanities), Sri Manakula Vinayagar Engg. College, Madagadipet, Puducherry 605 107, India
[d] Department of Physics, Bishop Moore College, Mavelikara, Kerala, India
[e] Centre for Molecular and Biophysics Research, Department of Physics, Mar Ivanios College, Thiruvananthapuram 695 015, Kerala, India
[f] Department of Physics, Women's Christian College, Nagercoil, Tamil Nadu, India
[g] Department of Inorganic Chemistry, Faculty of Science, Charles University in Prague, Albertov 2030, 128 40 Prague 2, Czech Republic

HIGHLIGHTS

- Vibrational spectral investigation of ADQF was carried out.
- Charge transfer interaction was analysed.
- N–H···O and C–H···O hydrogen bonding was identified.
- The HOMO–LUMO are also analysed.

GRAPHICAL ABSTRACT

Vibrational analysis of the 7-Amino-2,4-dimethylquinolinium formate (ADQF) molecule was carried out using FT-IR and FT-Raman spectroscopic techniques. The equilibrium geometry, harmonic vibrational wavenumbers, various bonding features have been computed using density functional method. The calculated molecular geometry parameters have been compared with XRD data. The detailed interpretation of the vibrational spectra has been carried out by computing Potential Energy Distribution (PED). Stability of the molecule arising from hyperconjugative interactions, charge delocalization have been analysed using Natural Bond Orbital (NBO) analysis. The simulated spectra satisfactorily coincide with the experimental spectra.
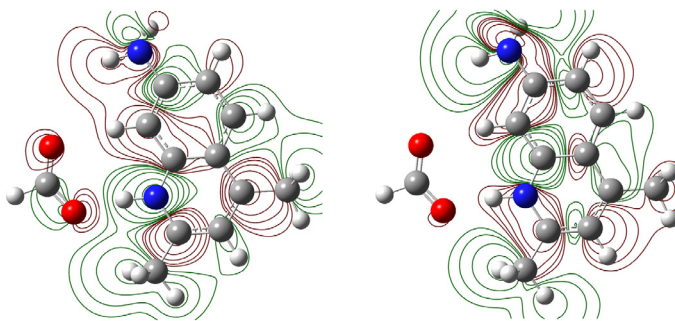
MO Contour plot

ARTICLE INFO

ABSTRACT

The molecular geometry, the normal mode frequencies and corresponding vibrational assignments, natural bond orbital analysis and the HOMO–LUMO analysis of 7-Amino-2,4-dimethylquinolinium formate in the ground state were performed by B3LYP levels of theory using the 6-31G(d) basis set. The optimised bond lengths and bond angles are in good agreement with the X-ray data. The vibrational spectra of the title compound which is calculated by DFT method, reproduces vibrational wave numbers and intensities

* Corresponding author. Tel.: +91 9940347178.
  E-mail address: nathan.amalphysics@gmail.com (M. Amalanathan).

with an accuracy which allows reliable vibrational assignments. The possibility of N–H···O hydrogen bonding was identified using NBO analysis. Natural bond orbital analysis confirms the presence of intra-molecular charge transfer and the hydrogen bonding interaction.

Introduction

The theoretical *ab initio* and Density Functional Theory (DFT) studies give information regarding the structural parameters, the functional groups, orbital interactions and vibrational frequencies. Hence, the investigation on the structure and fundamental vibrations of quinoline and its derivatives are still being carried out, increasingly [1–12]. The substituent's effect in quinoline ring leads to the variation of charge distribution in the molecule, and consequently, this greatly affects the structural, electronic and vibrational parameters. Quinolines are interesting because of their potential uses in medicines, Quinoline and its derivatives are of great interest in pharmacy, and some of them are used as antimalarial drugs [13]. It is also immensely used as a reagent in analytical chemistry. In spite of its above-mentioned importance, vibrational spectroscopic studies on quinoline are not plentiful [14,15]. The structural characteristics and vibrational spectroscopic analysis of the Pharmaceutical compound under investigation, 7-Amino-2,4-dimethylquinolinium formate (ADQF) has not been studied. Thus, owing to the industrial and biological importance of substituted quinolines, an extensive spectroscopic study on ADQF was carried out using Fourier transform infrared (FTIR) and FT-Raman spectra. The density functional theory is a popular post-HF approach for the calculation of molecular structures, vibrational frequencies and energies of molecules [16]. The DFT calculations with the hybrid exchange-correlation functional B3LYP (Becke's three parameter (B3) exchange in conjunction with the Lee–Yang–Parr's (LYP) correlation functional) which are especially important in systems containing extensive electron conjugation and/or electron lone pairs [17–20]. Therefore the present investigation has been undertaken to study the vibrational spectra of this molecule completely and to identify the various modes with greater wave number accuracy. Density Functional Theory (DFT) calculation has been performed to compute the vibrational wave number [19]. The Natural Bond Orbital (NBO) analysis explains the most important orbital interactions in order to clarify general structural features. The Mullikan population analysis and the HOMO–LUMO energy are also calculated.

Experimental

The infrared spectrum of the sample was recorded between 4000 and 400 cm^{-1} on a Mattson 1000 FT-IR spectrometer which was calibrated using polystyrene bands. The sample was prepared as a KBr disc. The FT-Raman spectrum of the sample was recorded between 3500 and 50 cm^{-1} regions on a Bruker FRA 106/S FT-Raman instrument using 1064 nm excitation from an Nd:YAG laser. The detector is a liquid nitrogen cooled Ge detector.

Computational details

The density functional theory [21] with the three-parameter hybrid functional (B3) [22] for the exchange part and the Lee–Yang–Parr (LYP) correlation function [23], level *ab initio* calculations have been carried out in the present investigation, using 6-31G(d) and 6-31++G(d,p) basis set with Gaussian 09 [24] program package. From that the optimised structure and the vibrational frequencies were

calculated. The binding energy (*E*) was calculated at the 6-31++G(d,p) level with correction for the Basis Set Superposition Error (BSSE) using the counterpoise method [25]. The use of finite basis in the calculation of molecular clusters by means of *ab initio* method is responsible of what is known as Basis Set Superposition Error (BSSE) [26,27]. This error is derived from the effective larger basis set used to compute the monomers within the complexes than the one used in the isolated monomers. Thus, the energy of the complex is overestimated with respect to the isolated monomers. The effect of the BSSE in weak interactions can be very important [28]. Thus, a large number of studies have been devoted to deal with this issue [29]. The most common method to evaluate the BSSE is the full counterpoise method (CP) which evaluates the energy of the monomers with the full basis set of the complex [30]. The 6-31++G(d,p) basis set was chosen for being one of the most popular basis sets used in the study of medium and large sized hydrogen bonded systems, and also for yielding a very small BSSE [31] with Counterpoise-corrected values. The calculated 6-31++G(d,p) basis set counterpoise corrected energy is −725.7960 Hartree and the counterpoise BSSE energy is 0.001202 Hartree. The optimised structural parameters are used in the vibrational frequency calculations at the DFT levels to characterise all stationary points as minima. Then vibrationally averaged nuclear positions of the compound ADQF are used for harmonic vibrational frequency calculations resulting in IR and Raman frequencies together with intensities. Owing to the complexity of the molecule, the Potential Energy Distribution (PED) is carried out to obtain complete information of the molecular motions involved in the normal modes of ADQF. The experimentally observed spectral data of the compound ADQF is found to be in good agreement with the spectral data obtained by quantum chemical calculations.

The vibrational modes are assigned on the basis of PED (Potential Energy Distribution) analysis using VEDA (Vibrational Energy Distribution Analysis) program [32]. The calculated vibrational wave numbers are scaled [33] with the scale factors in order to figure out how the calculated data are in agreement with those of the experimental ones. The calculated vibrational frequencies is scaled down by using the scaling factor 0.9613 [33] to offset the systematic error caused by neglecting anharmonicity and electron density. The calculated Raman activities (S_i) have been converted to relative Raman intensities (I_i) using the following relationship derived from the basic theory of Raman scattering [34,35]

$$I_i = \frac{f(v_o - v_i)^4 S_i}{v_i \left[1 - \exp\left(\frac{-hcv_i}{kT} \right) \right]} \tag{1}$$

where v_o is the exciting frequency (in cm^{-1} units), v_i the vibrational wave number of the *i*th normal mode, *h*, *c* and *k* the universal constants, and *f* is the suitably chosen common scaling factor for all the peak intensities.

Results and discussion

Molecular geometry

The optimized molecular structures of ADQF is shown in Fig. 1. The X-ray structure of ADQF molecule has been reported
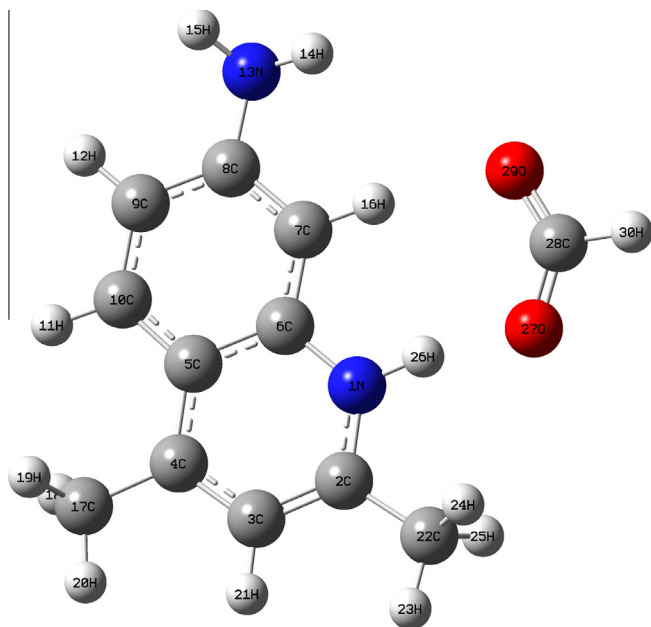
Fig. 1. Optimised molecular structure of ADQF.

previously [36]. Crystal structure parameters is triclinic, the space group $p\bar{1}$, with the unit-cell dimensions a = 7.2254 (19) Å, b = 9.167 (3) Å, c = 9.3662 (19) Å, α = 66.70 (3)° and β = 89.88 (3)°. The structure parameters obtained by X-ray single crystal diffraction method and it compares the calculated geometric parameters with the experimental data are given in Table 1. Based on this comparison, the calculated bond lengths and bond angles of ADQF show good agreement with the experimental data. As seen from Table 1, the

calculated geometric parameters represent good approximations to the XRD data on the whole. Most of the optimized bond lengths are slightly longer than the experimental values and the bond angles are slightly different from the experimental ones, because the molecular states are different in the experimental and theoretical processes. One isolated molecule is considered in gas phase in the theoretical calculation, while many packing molecules are treated in condensed phase in the experimental measurement.

It is observed that the influence of the substituent on the molecular parameters, particularly in the C–C bond distance of ring carbon atoms seems to be negligibly small except that C_2–C_3 (1.386 Å) and C_9–C_{10} (1.345 Å), where the CH_3 is attached with C4 and NH_2 is attached with C_8. All other C–C bond distances calculated are in the range 1.4021–1.4296 Å, which shows the substituent effect on the ring C–C bond. In ADQF the N–H bond length is measured as ~1.053 Å by DFT method and 0.99 Å by X-ray diffraction method, the H···O distance is about ~1.701 Å by DFT method and 1.69 Å by X-ray diffraction method. The above result confirms the possibility of intermolecular N–H···O hydrogen bond. With the electron donating substituents on the benzene ring, the symmetry of the ring is distorted, yielding ring angles smaller than120° at the point of substitution and slightly larger than 120° at the ortho and meta positions [37]. The CCC bond angle where the CH_3 is connected, show 118.57° while the angle of carbon where the NH_2 group is linked, C_7–C_8–C_9 is by 118.87°. The bond angle C_5–C_4–C_{17} is slightly lesser than that of C_3–C_4–C_{17} and is due to the steric repulsion between methyl group and the neighbouring hydrogen atom, like that bond angle C_7–C_8–C_{13} is slightly lesser than that of C_9–C_8–C_{13} and is due to the steric repulsion between NH_2 group and the neighbouring hydrogen atom. The equilibrium structure for the ground state shows that one of the methyl C–H bonds is parallel to the ring plane. In amino group, the nitrogen atom is slightly out-of-plane, with a torsional angle C_{22}–C_3–C_4–N_9 and C_6–C_5–C_4–N_9 in the ca. 177.5 (or ca. 2.5°). A measure of this displacement

Table 1
Optimized geometrical parameters of ADQF on B3LYP/6-31G(d) and B3LYP/631++G(d,p) level along with experimental.

Bond length	Value (Å)			Bond angle	Value (°)			Dihedral angle	Value (°)		
	Expt.	B3LYP/6-31G(d)	B3LYP/631++G(d,p)		Expt.	B3LYP/6-31G(d)	B3LYP/631++G(d,p)		Expt.	B3LYP/6-31G(d)	B3LYP/631++G(d,p)
N_1–C_2	1.327	1.3804	1.38	N_1–C_2–C_3	119.53	119.2	119.0	N_1–C_2–C_3–C_4	−1.25	−0.28	−0.2
C_2–C_3	1.386	1.3793	1.381	C_2–C_3–C_4	121.26	122.3	122.2	C_2–C_3–C_4–C_5	−1.71	−0.14	0
C_3–C_4	1.378	1.4112	1.414	C_3–C_4–C_5	118.57	118	118.0	C_{17}–C_4–C_5–C_6	177.92	179.78	−180
C_4–C_5	1.407	1.4425	1.442	C_4–C_5–C_6	119.23	118.7	118.6	C_{10}–C_5–C_6–C_7	−0.7	0.09	0
C_5–C_6	1.42	1.4341	1.435	C_5–C_6–C_7	121.97	121.3	121.3	N_1–C_6–C_7–C_8	−178.72	−179.43	−179.6
C_6–C_7	1.391	1.398	1.399	C_6–C_7–C_8	120.04	120.2	120.2	C_4–C_5–C_{10}–C_9	179.97	179.48	180
C_7–C_8	1.373	1.402	1.403	C_7–C_8–C_9	118.87	119.7	119.7	C_3–C_4–C_5–C_{10}	−179.97	−179.03	−179.4
C_8–C_9	1.429	1.4008	1.402	C_8–C_9–C_{10}	120.94	120	119.9	C_4–C_5–C_{10}–H_{11}	−0.07	−0.43	−0.2
C_9–C_{10}	1.345	1.4001	1.403	C_9–C_{10}–H_{11}	119	118.9	118.8	N_{13}–C_8–C_9–H_{12}	1.25	−1.68	−1.7
C_{10}–H_{11}	0.93	1.0872	1.086	C_{10}–C_9–H_{12}	119.57	120.1	120.0	$H16$–C_7–C_8–N_{13}	−1.43	4.19	3.9
C_9–H_{12}	0.928	1.0892	1.088	C_7–C_8–N_{13}	122.34	119.4	119.2	C_7–C_8–N_{13}–H_{14}	0	−19.25	−18
C_8–N_{13}	1.355	1.4157	1.413	C_8–N_{13}–H_{14}	119.94	111.4	112.7	C_7–C_8–N_{13}–H_{15}	−179.99	−143.11	−145.7
N_{13}–H_{14}	0.86	1.0158	1.014	C_8–N_{13}–H_{15}	120.03	112.7	113.9	C_5–C_6–C_7–H_{16}	−179.41	178.09	178.6
N_{13}–H_{15}	0.86	1.0151	1.013	C_6–C_7–H_{16}	120.01	118.9	119.1	C_2–C_3–C_4–C_{17}	−176.9	−179.6	−179.7
C_7–H_{16}	0.93	1.0924	1.09	C_3–C_4–C_{17}	119.84	121.4	121.3	C_3–C_4–C_{17}–H_{18}	−129.54	−121.01	−120.8
C_4–C_{17}	1.501	1.5015	1.501	C_4–C_{17}–H_{18}	109.48	112.5	112.3	C_3–C_4–C_{17}–H_{19}	100.59	119.62	119.7
C_{17}–H_{18}	0.96	1.1032	1.103	C_4–C_{17}–H_{19}	109.48	112.5	112.3	C_3–C_4–C_{17}–H_{20}	−9.54	−0.68	−0.5
C_{17}–H_{19}	0.96	1.1034	1.103	C_4–C_{17}–H_{20}	109.45	111	110	N_1–C_2–C_3–H_{21}	178.7	179.68	179.8
C_{17}–H_{20}	0.96	1.0968	1.096	C_2–C_3–H_{21}	119.38	118.3	118.2	C_6–$C1$–C_2–C_{22}	178.94	179.56	179.9
C_3–H_{21}	0.93	1.0888	1.088	N_1–C_2–C_{22}	117.05	116	116.2	C_3–C_2–C_{22}–H_{23}	42.17	−7.81	−1.3
C_2–C_{22}	1.493	1.5006	1.501	C_2–C_{22}–H_{23}	109.46	110.6	110.3	C_3–C_2–C_{22}–H_{24}	42.17	−129.38	−122.4
C_{22}–H_{23}	0.96	1.0954	1.094	C_2–C_{22}–H_{24}	109.49	111.2	108.9	C_3–C_2–C_{22}–H_{25}	162.16	112.98	162.6
C_{22}–H_{24}	0.96	1.0971	1.098	C_2–C_{22}–H_{25}	109.49	111.6	111.4	C_3–C_2–N_1–H_{26}	175.91	−0.28	179
C_{22}–H_{25}	0.96	1.0997	1.098	C_2–N_1–H_{26}	122.79	118.5	119.0	C_2–N_1–H_{26}–O_{27}	−20.01	−12.56	−6.5
N_1–H_{26}	0.989	1.0532	1.049	N_1–H_{26}–O_{27}	107.25	109.9	110.7	N_1–H_{26}–O_{27}–C_{28}	160.44	−161.95	−169.4
H_{26}–O_{27}	1.687	1.7019	1.719	H_{26}–O_{27}–C_{28}	123.87	124.4	125.4	H_{26}–O_{27}–C_{28}–O_{29}	166.71	−3.25	168.2
O_{27}–C_{28}	1.217	1.2668	1.27	O_{27}–C_{28}–O_{29}	129.55	130.1	128.9	H_{26}–O_{27}–C_{28}–H_{30}	12.26	176.81	14.3
C_{28}–O_{29}	1.21	1.2478	1.252	O_{27}–C_{28}–H_{30}	115.27	113.8	116.5				
C_{28}–H_{30}	0.93	1.1294	1.124								

Table 2
Second-order perturbation energy values between occupied and anti-bonding orbital of ADQF using NBO basis.

Donor (i)	ED (e)	Energy (i) (a.u.)	Acceptor (j)	ED (e)	Energy (j) (a.u.)	$E(2)^a$ (kJ mol^{-1})	$E(i)-E(j)^b$ (a.u.)	$F(I,j)^c$ (a.u.)
$\pi(C_4–C_5)$	0.8604	−0.09774	$\pi^*(C_2–C_3)$	0.1777	0.1725	73	709	234
$\pi(C_6–C_7)$	0.8636	−0.10359	$\pi^*(C_4–C_5)$	0.3800	0.1526	42	683	194
			$\pi^*(C_8–C_9)$	0.2127	0.1685	52	709	200
LP1N$_1$	0.8664	−0.10857	$\pi^*(C_2–C_3)$	0.1777	0.1725	70	735	231
			$\pi^*(C_6–C_7)$	0.1858	0.1809	87	761	263
LP1N$_{13}$	0.9460	−0.18018	$\pi^*(C_8–C_9)$	0.2127	0.1685	42	919	213
LP2O$_{27}$	0.9228	−0.11811	$\sigma^*(N_1–H_{26})$	0.0471	0.5963	62	1864	347
LP3O$_{27}$	0.8158	−0.05978	$\sigma^*(C_{28}–O_{29})$	0.0222	0.7582	215	656	378
LP2O$_{29}$	0.9337	−0.05837	$\sigma^*(C_{28}–H_{30})$	0.0471	0.5501	42	1602	260

[a] $E(2)$ means energy of hyperconjugative interactions; cf. Eq. (2).
[b] Energy difference between donor and acceptor i and j NBO orbitals.
[c] $F(i,j)$ is the Fock matrix element between i and j NBO orbitals.

is defined as the tilt angle [37]. Existence of this angle has been interpreted to be caused by asymmetric interaction between the NH$_2$ group and benzene ring plane.

NBO analysis

The Natural Bond Orbital (NBO) analysis has already been proved to be an effective tool for chemical interpretation of hyper conjugative interaction and electron density transfer from the filled lone pair electron. DFT level computation is used to investigate the various second order interaction between the filled orbitals of one subsystem and vacant orbitals of another subsystem, which is a measure of the delocalization or hyper conjugation [38]. The main natural orbital interactions are analyzed with the NBO 5.0 program [39]. The hyper conjugative interaction energy is deduced from the second-order perturbation approach

$$E(2) = -n_\sigma \frac{\langle\sigma|F|\sigma\rangle^2}{\varepsilon_{\sigma*} - \varepsilon_\sigma} = -n_\sigma \frac{F_{ij}^2}{\Delta E} \qquad (2)$$

where $\langle\sigma|F|\sigma\rangle^2$, or F_{ij}^2 is the Fock matrix element between i and j NBO orbitals, ε_σ and ε_σ^* are the energies of σ and σ^* NBO's, and n_σ is the population of the donor σ orbital.

The lowering of orbital energy due to the interaction between doubly occupied orbitals and unoccupied ones is a very convenient guide to interpret the molecular structure in the electronic point of view. In energetic terms, hyper conjugation is an important effect [40,41] in which an occupied Lewis-type natural bond orbital is stabilized by overlapping with a non-Lewis-type orbital (either one-centre Rydberg or two-centre anti-bonding NBO). This electron delocalization can be described as a charge transfer from a Lewis valence orbital (donor), with a decreasing of its occupancy, to a non-Lewis orbital (acceptor).

Table 2 shows the most important interactions between Lewis and non-Lewis orbitals with N and O lone pairs, the second-order perturbation energy values, $E(2)$, corresponding to these interactions, and the overlap integral of each orbital pair. A very strong interaction has been observed between the p type orbital containing the lone electron pair of N$_1$ and the neighbour $\pi^*(C_2–C_3)$, $\pi^*(C_6–C_7)$ anti-bonding orbital of the benzene ring. This interaction is responsible for a pronounced decrease of the lone pair orbital occupancy anti-bonding C$_2$–C$_3$ (0.177e), C$_6$–C$_7$ (0.1809e) than the other C–C occupancy, and is possible to charge transfer N$_1$ from in the benzene ring, which is a common molecular feature of this type of Pharmaceutical compound, which interaction is responsible for the Pharmaceutical activity of the ADQF compound. This interaction is confirmed from the shortening of bond length N$_1$–C$_2$ (1.380 Å) and N$_1$–C$_6$ (1.380 Å) from the normal value. The intermolecular hyper conjugative interactions are formed by the orbital overlap between $\pi(C–C)$ and $\pi(C–C)$ bond orbitals, which results intramolecular

charge transfer (ICT) causing stabilization of the system. The orbital interaction energy between $\pi(C_4–C_5) \rightarrow \pi^*(C_2–C_3)$, $\pi(C_6–C_7) \rightarrow \pi^*(C_4–C_5)$, $\pi(C_6–C_7) \rightarrow \pi^*(C_8–C_9)$ and $\pi(C_8–C_9) \rightarrow \pi^*(C_6–C_7)$ are 73.3, 41.8, 52.0 and 25.3 kJ mol^{-1}, respectively (Table 2). These increasing interaction energies are due to the strong ICT interactions leading to stabilization of the molecule.

The importance of hyper conjugative interaction and electron density transfer (EDT) from filled lone electron pairs of the LP(Y) of the "Lewis base" Y into the unfilled anti-bond $\sigma^*(X–H)$ of the "Lewis acid" X–H in X–H···Y hydrogen bonding system have been already reported [42]. The intermolecular N–H···O hydrogen bonding is formed due to the orbital overlap between the LP2O$_{27}$ and $\sigma^*(N_1–H_{26})$ which results ICT causing stabilization of the H-bonded systems. Thus the nature and strength of the intermolecular hydrogen bonding can be explored by studying the changes in electron densities in vicinity of N–H hydrogen bonds. Hydrogen bonding interaction leads to an increase in electron density (ED) of N–H anti-bonding orbital. The increase of population in N–H anti-bonding orbital weakens the N–H bond. The NBO analysis of ADQF clearly shows the evidences of the formation H-bonded interaction between oxygen lone electron pairs and $\sigma^*(N–H)$ anti-bonding orbital having the stabilization energy 62.2 kJ mol^{-1}. The magnitudes of charges transferred from lone pairs of LP2O$_{27}$ of the hydrogen bonded O atoms into the anti-bonds $\sigma^*(N_1–H_{26})$ being the H-donors is significantly increased (0.04717e) upon adding hydrogen bonded in ADQF unambiguous evidence about the weakening of both bonds, their elongation and concomitant red shifts of their stretching frequencies. The stabilization energy $E(2)$ associated with hyper conjugative interactions LP2O$_{27}$ and $\sigma^*(N_1–H_{26})$ is obtained as 62.2 kJ mol^{-1}, which quantify the extend of hydrogen bonding between the LP2O$_{27}$ and $\sigma^*(N_1–H_{26})$. The differences in $E(2)$ energies are possibly due to the fact that the accumulation of electron density in the N–H bond is not only drawn from the LP O of hydrogen-acceptor but also from the entire molecule, which leads to bond weakening and its elongation of N$_1$–H$_{26}$ (1.053 Å) bond from the normal value. An important contribution for the molecular stabilization is further given by O$_{29}$ through the overlap of lone pair n(LP3 O$_{27}$) with the $\sigma^*(C_{28}–O_{27})$ orbital. The energy contribution of LP2O$_{29} \rightarrow \sigma^*(C_1–H_{16})$ values is 41.8 kJ mol^{-1}. These energy $E(2)$ values are chemically significant and can be used as a measure of the intramolecular C–H···O hydrogen bonding interaction between the oxygen lone-pair and the anti-bonding orbitals.

Vibrational analysis

The vibrational spectral analysis is performed on the basis of the characteristic vibrations of the amino group, hydroxyl group, carbonyl group and methyl group. The computed wave numbers,
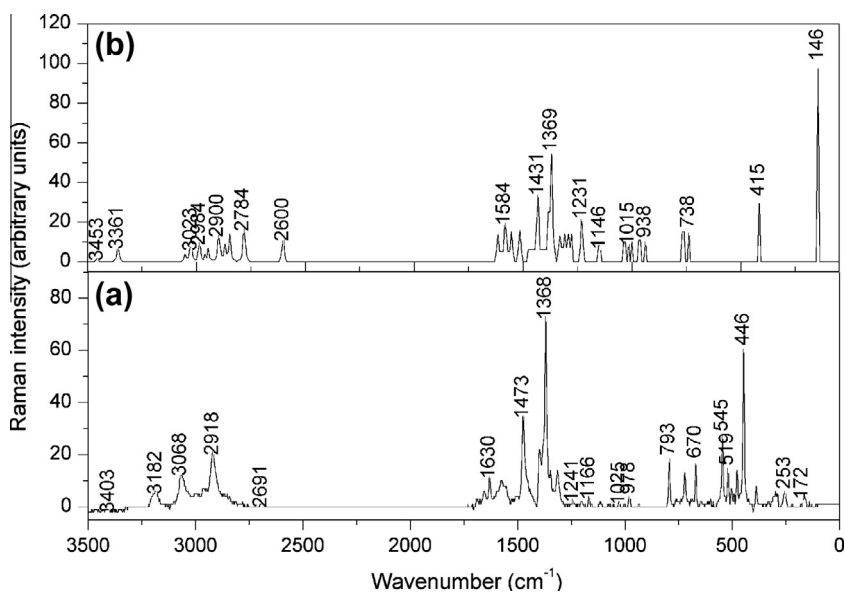
Table 3
Calculated and observed vibrational frequencies for ADQF and their tentative assignment.

ν_{cal} (cm^{-1})		ν_{IR} (cm^{-1})	ν_{Raman} (cm^{-1})	Assignment PED (%)
31G(d)	631++G(d,p)			
3461	3503	3367 s	3483 w	N$_{13}$–H$_{14}$ stretch (53%) + N$_{13}$–H$_{15}$ stretch (45%)
3367	3402	3173 s	3183 w	N$_{13}$–H$_{14}$ stretch (46%) + N$_{13}$–H$_{15}$ stretch (53%)
3058	3063	–	3069 m	C$_9$–H$_{12}$ stretch (11%) + C$_{10}$–H$_{11}$ stretch (89%)
3038	3040		–	C$_3$–H$_{21}$ stretch (99%)
3028	3031	–	–	C$_9$–H$_{12}$ stretch (89%) + C$_{10}$–H$_{11}$ stretch (11%)
2996	3008	–	–	C$_{22}$–H$_{23}$ stretch (42%) + C$_{22}$–H$_{24}$ stretch (16%) + C$_7$–H$_{16}$ stretch (40%)
2990	2988	–	–	N$_{13}$–H$_{14}$ stretch (46%) + N$_{13}$–H$_{15}$ stretch (53%) + C$_{22}$–H$_{23}$ stretch (30%) + C$_7$–H$_{16}$ stretch (59%)
2966	2960	2916 w	2920 m	C$_{17}$–H$_{20}$ stretch (91%)
2953	2940	–	–	C$_{22}$–H$_{24}$ stretch (60%) + C$_{22}$–H$_{25}$ stretch (53%) + C$_{22}$–H$_{23}$ stretch (23%)
2903	2900	–	–	C$_{22}$–H$_{25}$ stretch (70%) + C$_{22}$–H$_{24}$ stretch (13%) + C$_{22}$–H$_{23}$ stretch (14%)
2876	2859	–	2850 w	C$_{17}$–H$_{18}$ stretch (51%) + C$_{17}$–H$_{19}$ stretch (47%)
2854	2845	–	–	C$_{17}$–H$_{19}$ stretch (48%) + C$_{17}$–H$_{18}$ stretch (43%)
2753	2836	2781 m	–	N$_1$–H$_{26}$ stretch (93%)
2610	2656	2696 m	2699 vw	C$_{28}$–H$_{30}$ stretch (97%)
1672	1623	1648 vs	1655 w	O$_{29}$–C$_{28}$ stretch (46%) + O$_{27}$–C$_{28}$ stretch (28%) + H$_{26}$–N$_1$–C$_6$ bend (11%)
1623	1592	1629 vs	1630 m	O$_{27}$–C$_{28}$ stretch (46%) + H$_{26}$–N$_1$–C$_6$ bend (39%) + N$_1$–H$_{26}$–O$_{27}$ bend (13%)
1619	1591	–	–	H$_{14}$–N$_{13}$–H$_{15}$ bend (78%)
1586	1574	1596 vvs	1576 m	C$_2$–C$_3$ stretch (14%) + C$_6$–C$_7$ stretch (17%) + C$_8$–C$_9$ stretch (15%)
1561	1549	1513 m	–	C$_2$–C$_3$ stretch (17%) + C$_7$–C$_8$ stretch (22%) + H$_{16}$–C$_7$–C$_8$ bend (14%)
1521	1503	1478 w	1473 s	C$_5$–C$_{10}$ stretch (19%) + H$_{11}$–C$_{10}$–C$_9$ bend (15%)
1479	1453		–	H$_{21}$–C$_3$–C$_2$ bend (24%) + N$_1$–C$_2$ stretch (14%) + C$_3$–C$_4$ stretch (16%)
1463	1439	1463 m	–	C$_{22}$–H$_{24}$–C$_2$–H$_{25}$ out (10%) + H$_{18}$–C$_{17}$–H$_{19}$ bend (11%) + H$_{24}$–C$_{22}$–C$_2$ bend (13%) + H$_{24}$–C$_{22}$–H$_{25}$ bend (36%)
1443	1422	1432 w	–	C$_{17}$–H$_{19}$–C$_4$–H$_{20}$ out (11%) H$_{18}$–C$_{17}$–H$_{20}$ bend (84%)
1440	1417	1397 w	1398 w	H$_{24}$–C$_{22}$–C$_2$ bend (12%) + H$_{23}$–C$_{22}$–C$_2$–C$_3$ tors (26%)
1439	1412	–	–	H$_{23}$–C$_{22}$–C$_2$–C$_3$ tors (21%) + H$_{24}$–C$_{22}$–C$_2$–C$_3$ tors (18%)
1420	1405	–	–	H$_{12}$–C$_9$–C$_{10}$ bend (11%) + H$_{11}$–C$_{10}$–C$_9$ bend (11%) + C$_7$–C$_8$ stretch (10%) + C$_6$–C$_7$ stretch (12%)
1388	1375		–	C$_{22}$–H$_{24}$–C$_2$–H$_{25}$ out (18%) + H$_{23}$–C$_{22}$–C$_2$ bend (20%) + H$_{24}$–C$_{22}$–H$_{25}$ bend (22%) + H$_{24}$–C$_{22}$–H$_{25}$ bend (22%)
1386	1367	1383 m	–	C$_{17}$–H$_{19}$–C$_4$–H$_{18}$ out (11%) + H$_{18}$–C$_{17}$–H$_{19}$ bend (47%) + H$_{20}$–C$_{17}$–C$_4$ bend (13%)
1376	1355	–	–	H$_{30}$–C$_{28}$–O$_{29}$ bend (66%)
1370	1339	–	–	H$_{30}$–C$_{28}$–O$_{29}$ bend (19%) + C$_{17}$–H$_{19}$–C$_4$–H$_{18}$ out (15%) + H$_{18}$–C$_{17}$–H$_{19}$ bend (14%) + H$_{20}$–C$_{17}$–C$_4$ bend (13%)
1334	1329	1337 s	1369 vvs	H$_{12}$–C$_9$–C$_{10}$ bend (11%) + H$_{11}$–C$_{10}$–C$_9$ bend (11%) + C$_7$–C$_8$ stretch (10%) + C$_6$–C$_7$ stretch (12%)
1323	1308	–	1346 m	O$_{27}$–C$_{28}$–O$_{29}$ bend (13%) + O$_{27}$–C$_{28}$ stretch (52%) + O$_{29}$–C$_{28}$ stretch (26%)
1316	1303	1314 m	1312 w	C$_3$–C$_4$ stretch (28%)
1296	1285	–	–	N$_1$–C$_6$ stretch (18%) + H$_{16}$–C$_7$–C$_8$ bend (18%) + H$_{12}$–C$_9$–C$_{10}$ bend (10%)
1237	1277	1242 m	1242 w	C$_5$–C$_{10}$ stretch (10%) + H$_{11}$–C$_{10}$–C$_9$ bend (12%)
1208	1224	1210 w	1199 w	N$_{13}$–C$_8$ stretch (19%) + N$_1$–C$_6$ stretch (16%) + H$_{11}$–C$_{10}$–C$_9$ bend (20%)
1144	1198	1170 w	1167 w	C$_2$–C$_{22}$ stretch (12%) + C$_9$–C$_{10}$ stretch (16%) + H$_{21}$–C$_3$–C$_2$ bend (18%) + H$_{12}$–C$_9$–C$_{10}$ bend (12%)
1115	1147	–	–	H$_{14}$–N$_{13}$–C$_8$ bend (45%) + H$_{12}$–C$_9$–C$_{10}$ bend (10%)
1087	1104	–	1115 w	H$_{14}$–N$_{13}$–C$_8$ bend (10%) + C$_9$–C$_{10}$ stretch (31%) + H$_{12}$–C$_9$–C$_{10}$ bend (25%)
1039	1088	1077 w	1078 w	C$_4$–C$_{17}$ stretch (20%) + H$_{20}$–C$_{17}$–C$_4$ bend (17%)
1029	1034	1033 w	1027 w	H$_{14}$–N$_{13}$–C$_8$ bend (66%) + H$_{23}$–C$_{22}$–C$_2$–C$_3$ tors (17%)
1025	1013	–	–	C$_{28}$–O$_{27}$–O$_{29}$–H$_{30}$ out (93%)
1014	1011	–	–	H$_{18}$–C$_{17}$–H$_{20}$ bend (11%) + C$_{17}$–H$_{19}$–C$_4$–H$_{20}$ out (77%)
1009	998	–	–	H$_{23}$–C$_{22}$–C$_2$ bend (32%) + C$_{22}$–H$_{24}$–C$_2$–H$_{25}$ out (21%)
966	997	1001 vw	1001 w	C$_8$–C$_9$ stretch (14%)
947	965	976 wv	980 w	C$_2$–N$_1$–H$_{26}$–O$_{27}$ tors (39%) + H$_{26}$–N$_1$–C$_2$–C$_3$ out (20%)
943	946	935 w	936 w	C$_{17}$–H$_{19}$–C$_4$–H$_{18}$ out (21%) + C$_3$–C$_4$ stretch (16%) + H$_{20}$–C$_{17}$–C$_4$ bend (16%)
912	905	887 vw	–	C$_7$–C$_6$–C$_8$–H$_{16}$ out (63%) + C$_7$–H$_{16}$–O$_{29}$–C$_{28}$ out (14%)
852	893	–	–	N$_1$–C$_2$ stretch (20%) + C$_2$–C$_{22}$ stretch (14%) + C$_7$–C$_8$ stretch (12%)
837	831	846 m	–	C$_3$–C$_2$–N$_1$ bend (12%) + C$_2$–N$_1$–C$_6$ bend (33%) + C$_7$–C$_6$–N$_1$ bend (11%)
816	797	834 m	–	H$_{12}$–C$_9$–C$_8$–N$_{13}$ tors (11%) + H$_{11}$–C$_{10}$–C$_9$–N$_{12}$ tors (82%)
803	755	–	–	H$_{21}$–C$_3$–C$_4$–C$_{17}$ tors (79%)
766	746	791 m	793 m	N$_{13}$–H$_{14}$–C$_8$–H$_{15}$ out (42%) + H$_{12}$–C$_9$–C$_8$–N$_{13}$ tors (21%)
740	724	761 w	759 w	N$_{13}$–H$_{14}$–C$_8$–H$_{15}$ out (12%) + H$_{21}$–C$_3$–C$_4$–C$_{17}$ tors (40%) + C$_5$–C$_6$–C$_7$–C$_8$ tors (32%)
735	716	–	–	O$_{27}$–C$_{28}$–O$_{29}$ bend (78%)
707	697	720 w	721 m	H$_{12}$–C$_9$–C$_8$–N$_{13}$ tors (40%) + C$_5$–C$_6$–C$_7$–C$_8$ tors (19%)
699	664	–	–	C$_5$–C$_6$ stretch (15%) + C$_3$–C$_2$–N$_1$ bend (12%) + C$_5$–C$_{10}$–C$_9$ bend (15%)
683	649	666 w	666 m	N$_{13}$–C$_8$ stretch (16%) + C$_8$–C$_9$–C$_{10}$ bend (19%)
633	591	–	646 w	C$_4$–C$_{17}$ stretch (10%) + N$_{13}$–C$_8$ stretch (18% + C$_3$–C$_4$–C$_5$ bend (12%) + C$_3$–C$_2$–N$_1$ bend (10%)
595	541	595 m	–	C$_8$–C$_7$–C$_6$–N$_1$ tors (17%) + C$_7$–C$_8$–C$_9$–C$_{10}$ tors (40%) + C$_6$–C$_7$–C$_8$–C$_{13}$ tors (10%)
540	521	539 w	546 w	C$_3$–C$_2$–N$_1$–C$_6$ tors (13%) + C$_4$–C$_3$–C$_2$–N$_1$ tors (53%)
500	492	–	518 w	C$_7$–C$_6$–N$_1$ bend (10%) + C$_5$–C$_4$–C$_{17}$ bend (21%) + C$_3$–C$_2$–C$_{22}$ bend (27%)
487	481	–	500 w	C$_5$–C$_{10}$–C$_9$–C$_8$ tors (29%) + C$_3$–C$_2$–N$_1$–C$_6$ tors (29%)
476	459	476 w	477 w	C$_7$–C$_6$–N$_1$ bend (11%) + C$_7$–C$_8$–N$_{13}$ bend (13%)
448	422	449 w	445 vs	C$_6$–C$_7$ stretch (10%) + C$_7$–C$_8$–C$_9$ bend (23%) + C$_5$–C$_{10}$–C$_9$ bend (10%)
400	389	–	–	C$_5$–C$_{10}$–C$_9$–C$_8$ tors (35%) + C$_3$–C$_2$–N$_1$–C$_6$ tors (11%) + C$_5$–C$_6$–C$_7$–C$_8$ tors (12%)
365	345	–	–	C$_3$–C$_4$–C$_5$ bend (15%) + C$_3$–C$_2$–N$_1$ bend (14%) + C$_7$–C$_8$–N$_{13}$ bend (23%) + C$_3$–C$_2$–C$_{22}$ bend (11%)
287	283	–	388 w	C$_7$–C$_8$–C$_9$–C$_{10}$ tors (13%) + C$_6$–C$_7$–C$_8$–N$_{13}$ tors (13%) + C$_4$–C$_3$–C$_2$–C$_{22}$ tors (26%)
284	267	–	283 w	C$_7$–C$_8$–N$_{13}$ bend (19%) + C$_5$–C$_4$–C$_{17}$ bend (17%) + C$_3$–C$_2$–C$_{22}$ bend (14%)
267	263	–	253 w	H$_{14}$–N$_{13}$–C$_8$–C$_7$ tors (81%)
240	229	–		C$_7$–C$_6$–N$_1$ bend (16%) + C$_5$–C$_4$–C$_{17}$ bend (28%)
231	216	–	–	C$_8$–C$_7$–C$_6$–N$_1$ tors (36%) + C$_2$–N$_1$–C$_6$–C$_7$ tors (10%) + C$_6$–C$_7$–C$_8$–N$_{13}$ tors (21%)
197	198	–	220 w	C$_2$–C$_3$–C$_4$–C$_{17}$ tors (27%) + C$_4$–C$_3$–C$_2$–C$_{22}$ tors (19%) + C$_6$–C$_7$–C$_8$–N$_{13}$ tors (10%) + H$_{19}$–C$_{17}$–C$_4$–C$_3$ tors (19%)

Table 3 (continued)

ν_{cal} (cm^{-1})		ν_{IR} (cm^{-1})	ν_{Raman} (cm^{-1})	Assignment PED (%)
31G(d)	631++G(d,p)			
184	170	–	178 w	O$_{27}$–H$_{26}$ stretch (80%)
173	162	–	164 w	H$_{19}$–C$_{17}$–C$_4$–C$_3$ tors (65%) + H$_{26}$–O$_{27}$–C$_{28}$–O$_{29}$ tors (11%)
157	120		142 w	H$_{26}$–O$_{27}$–C$_{28}$–O$_{29}$ tors (63%)
116	115	–	–	H$_{26}$–O$_{27}$–C$_{28}$ bend (70%)
108	99	–	–	C$_2$–C$_3$–C$_4$–C$_{17}$ tors (20%) + H$_{23}$–C$_{22}$–C$_2$–C$_3$ tors (12%) + H$_{24}$–C$_{22}$–C$_2$–C$_3$ tors (23%) + C$_3$–C$_2$–N$_1$–C$_6$ tors (11%)
98	98	–	–	H$_{24}$–C$_{22}$–C$_2$–C$_3$ tors (32%)
94	94	–	–	C$_4$–C$_3$–C$_2$–C$_{22}$ tors (12%) + C$_2$–N$_1$–C$_6$–C$_7$ tors (41%) + C$_6$–C$_7$–C$_8$–N$_{13}$ tors (15%)
65	54	–	–	H$_{26}$–N$_1$–C$_6$ bend (14%) + N$_1$–H$_{26}$–O$_{27}$ bend (55%) + H$_{26}$–O$_{27}$–C$_{28}$ bend (13%)
44	42	–	–	C$_7$–C$_6$–C$_8$–H$_{16}$ out (11%) + C$_7$–H$_{16}$–O$_{29}$–C$_{28}$ out (52%)
36	37	–	–	H$_{26}$–N$_1$–C$_2$–C$_3$ out (51%) + C$_2$–N$_1$–H$_{26}$–O$_{27}$ tors (22%)
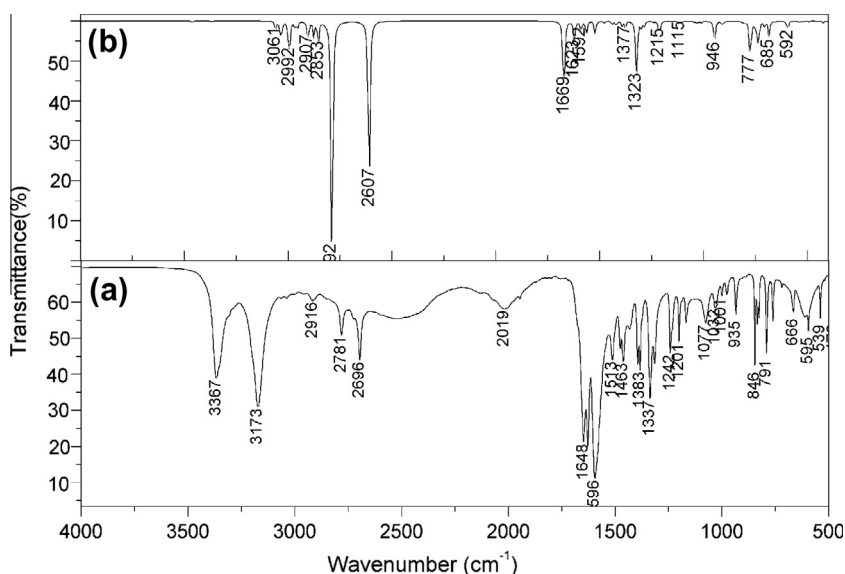
Fig. 2. (a) Experimental and (b) simulated FT-IR spectra of ADQF in the range 4000–400 cm^{-1}.

Fig. 3. (a) Experimental and (b) simulated FT-Raman spectra of ADQF in the range 3500–50 cm^{-1}.

their IR intensities and Raman activity corresponding to different modes are listed in Table 3 along with detailed assignments. The observed and simulated FT-IR and Raman spectra and selected vibrational normal modes are shown in Figs. 2 and 3.

Amino group vibrations

The fundamental modes involving the amino group are stretching and bending of NH bonds, torsion and inversion. The title molecule under investigation possesses one NH_2 group and hence one expects one symmetric and one asymmetric N–H stretching vibrations. In all the primary aromatic amines the N–H stretching frequency occurs in the region 3300–3500 cm^{-1} [43,44]. The antisymmetric ν_{as} stretching mode appears to be higher wave number than the symmetric ν_s. In ADQF the NH_2 asymmetric stretching vibration is observed in IR at 3367 as a medium band, the symmetric stretching vibration is observed in IR at 3173 cm^{-1} and in Raman at 3183 cm^{-1}. The frequency lowering present in the molecule is due the intermolecular interaction. The characteristic frequency of the NH_2 scissoring vibration is usually located in the range 1650–1600 cm^{-1}. The very strong band observed in IR at 1596 cm^{-1} and weak band observed in Raman at 1576 cm^{-1} is assigned to the NH_2 scissoring vibration. The other NH_2 bending modes are tabulated.

Methyl group vibration

Methyl group vibrations are generally referred to as electron donating substituent in the aromatic rings system, the asymmetric C–H stretching mode of CH_3 is expected around 2980 cm^{-1} and the CH_3 symmetric stretching is expected at 2870 cm^{-1} [45,46]. The Me1 asymmetric stretching is observed as weak band in Raman at 2850 cm^{-1}. The symmetric stretching mode of Me1 is observed 2781 cm^{-1} in IR. The shifting of the methyl stretching wave number is due to the influence of electronic effect resulting from the hyper conjugation and induction of methyl group in the aromatic ring [47]. Hyper conjugation causes the interaction of the orbital of the methyl group with π orbital of an aromatic ring system [47]. The asymmetric bending of Me2 is observed at 1397 cm^{-1} in IR and at 1398 cm^{-1} in Raman as a medium band. The asymmetric bending of Me1 is observed at 1383 cm^{-1} in IR as a medium band. These characteristic frequencies are in close agreement with those reported for the similar compounds [48]. The Band observed at 935 cm^{-1} in IR and 936 cm^{-1} in Raman is CH_3 out of plane bending modes. The bonds at 283 cm^{-1} in FT-Raman are assigned to methyl twisting mode.

Carbonyl group vibrations

The carbonyl group stretching vibrations give rise to the characteristic bands in IR and Raman. The intensity of these bands can increase because of the formation of hydrogen bonds. The carbonyl group vibration is observed in the region 1760–1730 cm^{-1} [49,50]. The strong band at 1648 cm^{-1} in IR and a weak band at 1655 cm^{-1} in Raman are assigned to carbonyl C_{28}–O_{29} stretching mode. The C_{28}–O_{27} stretching mode is observed in IR at 1629 cm^{-1} as a strong band and in Raman at 1630 cm^{-1} as a medium band. From that both C_{28}–O_{27}, and C_{28}–O_{29} stretching vibrations are lowering from the normal value. The red shifting of carbonyl stretching mode is attributed to the fact that the carbonyl group chelate with the other nucleophilic group, thereby forming both intra- and intermolecular hydrogen bonding in the crystal. The C_{28}–O_{27} stretching in lowering is due to the formation of N–H···O hydrogen bonding in the molecule. The C–O out of plane bending is identified as weak band in Raman at 142 cm^{-1}.

C–N vibrations

The ring C–N stretching vibration occurs in the region 1310–1290 cm^{-1} [43]. Thus, the bands observed at 1314 cm^{-1} (IR) and 1312 cm^{-1} (Raman) is from the ring C–N stretching. The C–N bending is observed in IR at 846 cm^{-1} as a weak band.

Ring vibration

The carbon–hydrogen stretching vibrations give rise to bands in the region 3000–3100 cm^{-1} in all aromatic compounds [51–53]. The intense band in Raman at 3069 cm^{-1} is assigned for ring C–H stretching wave number. The C–H in plane vibrations is appearing in the region 1000–1290 cm^{-1}. The strong band observed in IR at 1337 cm^{-1} and in Raman at 1369 cm^{-1} is assigned the C–H in plane bending of ADQF. The series of bands observed in IR at 1170 and 1033 cm^{-1} and in Raman at 1199, 1167, 1115 and 1027 cm^{-1} are assigned to the ring C–H in plane bending ring. The C–H out of plane vibration of the ring is observed in the region 770–730 cm^{-1} and for the tri substituted ring is 800–760 cm^{-1}. In ADQF the C–H out of plane vibration are observed in IR at 834, 791 cm^{-1} as medium band and is observed in Raman at 793 as a medium band. The C_3–H_{21} stretching is observed as a weak band IR at 2916 cm^{-1} and as medium band in Raman at 2920 cm^{-1}. The C_3–H_{21} out of plane bending is observed at 761 cm^{-1} as a weak band in IR and Raman.

The ring C–C stretching vibration occurs in the region 1625–1430 cm^{-1} [50]. For six membered aromatic rings, there are two or three bands in this region due to skeletal vibration; the strongest usually being about 1500 cm^{-1}. In the case where the ring is conjugated further, a band is about 1580 cm^{-1}. The C–C stretching of ring is observed at 1513 cm^{-1} in IR as a medium band. The same band is observed in IR at 1478 cm^{-1} as a weak band and in Raman at 1473 cm^{-1} as the strong band. The aromatic ring deformation vibrations appear in the region of 625–605 cm^{-1} for the mono substituted ring and 475–425 cm^{-1} for the trisubstituted ring. The series of weak band observed in IR at 666, 595, 539, 449 cm^{-1} and medium to strong band in Raman at 666, 546, 445 cm^{-1} are assigned to the C–C ring deformation.

Low-wave number hydrogen-bond vibrations

The attractive interaction between the hydrogen donor group and the acceptor moiety leads to the occurrence of new vibrational degrees of freedom, the so-called hydrogen bond modes. Such modes are connected with elongations changing the A···B distance and/or the relative orientation of the hydrogen-bonded groups. Thus, they provide direct insight into the structure of the hydrogen bonds and into the processes of bond formation and cleavage. As such modes are characterized by a high reduced mass of the oscillator and a small force constant determined by the comparably weak attractive interaction along the hydrogen bond, hydrogen bond modes [54] occur at low wave numbers in the range between 50 and 300 cm^{-1}. An interesting feature of these vibrations is the occurrence of an intense Raman band in the low-wave number region 164 cm^{-1} corresponding to the H···O stretching. This shows that there is a possibility of N–H···O hydrogen bonding present in the ADQF molecule.

HOMO–LUMO energy gap

In principle, there are several ways to calculate the excitation energies. The first, and the simplest one, involves the difference between the highest occupied molecular orbital (HOMO) and the lowest unoccupied molecular orbital (LUMO) of a neutral system. This form corresponds to the frozen orbital approximation, as the ground state properties are used to calculate excitation values. The HOMO–LUMO energy gap for ADQF has been calculated DFT level. The Eigen values of LUMO–HOMO energy gap reflect the
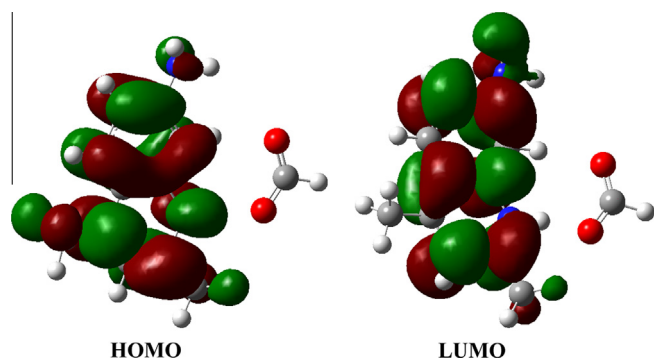
HOMO   **LUMO**

Fig. 4. HOMO and LUMO plot of ADQF.

chemical activity of the molecule. The atomic orbital compositions of the molecular orbitals are sketched in Fig. 4. The calculated energies and the energy gap is

HOMO energy $= -6.019$ eV

LUMO energy $= -4.474$ eV

HOMO$-$LUMO energy gap $= 1.544$ eV

The decrease in the HOMO and LUMO energy gap explains the eventual charge transfer interaction taking place within the molecule, due to the strong electron-accepting ability of the electron-acceptor group. It is worth noting that HOMOs have an overall π bonding character along with a considerable non-bonding character and LUMOs have an anti-bonding π^* character. The strong charge transfer interaction is responsible for the bioactivity of the molecule.

Conclusion

A complete vibrational analysis of ADQF was performed using DFT calculations at B3LYP/6-31G* and B3LYP/6-31++G** levels in order to elucidate the structural activity relationship. FT-IR and FT-Raman spectra have been recorded and the detailed vibrational assignments were presented. The molecular geometry, vibrational frequencies, infrared intensities and Raman intensities of ADQF in the ground state have been calculated by using density functional theory. The hydrogen bonds network has been thoroughly analyzed using NBO analysis. The transfer of ED from the lone pair oxygen to the anti-bonding orbital of N–H bond produces strong evidences for two hydrogen bonds. The molecular hydrogen bonding and charge transfer interaction present in the molecule gives the important of ADQF that brings about most interesting Pharmaceutical activity. The natural bond orbital analysis confirms the hyper conjugation interaction and the possibility of N–H$\cdots$O and C–H$\cdots$O interaction. The lowering of carbonyl mode and the low wave number hydrogen bonds shows the occurrence of N–H$\cdots$O hydrogen bonds. The assignment of most of the normal modes agrees well with the theoretical wave numbers. The HOMO–LUMO energy gap has a substantial influence on the ICT and the calculated value is found to be 1.544 eV. The lowering of HOMO–LUMO energy gap, a quantum–chemical descriptor, explains the charge transfer interactions taking place within the molecule through strong N–H$\cdots$O and C–H$\cdots$O hydrogen bonding which is prove that the ADQF is bioactive and pharmaceutical in nature.

References

[1] K. Bahgat, A.G. Ragheb, Cent. Eur. J. Chem. 5 (2007) 201–220.
[2] K. Arici, M. Yurdakul, S. Yrdakul, Spectrochim. Acta 61A (2005) 37–40.
[3] V. Krishnakumar, R. Ramasay, Spectrochim. Acta 61A (2005) 673–683.
[4] T. Dziembowska, M. Szafran, E. Jagodzinska, I. Natkaniec, A. Pawlukoj, J.S. Kwiatkowski, J. Baran, Spectrochim. Acta 59A (2003) 2175–2189.
[5] M.J. Mphahlele, A.M. El-Nahas, T.M. El-Gogary, J. Mol. Struct. 690 (2004) 151–157.
[6] A.E. Özel, Y. Büyükmurat, S. Akyüz, J. Mol. Struct. 455 (2001) 565–566.
[7] C. Engelter, G.E. Jackson, C.L. Knight, D.A. Thornton, J. Mol. Struct. 213 (1989) 133–144.
[8] L. Türker, Y. Yıldırır, J. Mol. Struct. Theochem. 676 (2004) 47–53.
[9] N. Tokay, C. Ögretir, J. Mol. Struct. Theochem. 594 (2002) 185–197.
[10] R. Zwaans, C. Thomson, J. Mol. Struct. Theochem. 362 (1996) 51–68.
[11] A.J. Camargo, H.B. Napolitano, J. Zukerman-Schpector, J. Mol. Struct. Theochem. 816 (2007) 145–151.
[12] M.A. Shashidar, K.S. Rao, Indian J. Phys. 41 (1967) 299.
[13] B.G. Katzung, Basic and Clinical Pharmacology, Appleton and Lange, Prentice-Hall, Lebanon, 1989.
[14] S.C. Wait, J.C. McNerney, J. Mol. Spectrosc. 34 (1970) 56–61.
[15] S.S. Singh, Labdev J. Sci. Technol. 10A (1972) 14–19.
[16] K. Golcuk, A. Altun, M. Kumru, Spectrochim. Acta 59A (2003) 1841–1847.
[17] M.E. Vaschetto, B.A. Retamal, A.P. Monkman, J. Mol. Struct. Theochem. 468 (1999) 209–221.
[18] Timothy Clark, Jayaraman Chandrasekhar, Günther W. Spitznagel, Paul Von Ragué Schleyer, J. Comput. Chem. 4 (1983) 294.
[19] Scott Gronert, Chem. Phys. Lett. 252 (1996) 415–418.
[20] D.A. Forsyth, A.B. Sebag, J. Am. Chem. Soc. 119 (1997) 9483–9494.
[21] A.D. Becke, J. Chem. Phys. 98 (1993) 5648.
[22] C. Lee, W. Yang, R.G. Parr, Phys. Rev. B 37 (1988) 785.
[23] P. Hohenberg, W. Kohn, Phys. Rev. 136 (1964) B864–B871.
[24] M.J. Frisch, G.W. Trucks, H.B. Schlegel, G.E. Scuseria, M.A. Robb, J.R. Cheeseman, G. Scalmani, V. Barone, B. Mennucci, G.A. Petersson, H. Nakatsuji, M. Caricato, X. Li, H.P. Hratchian, A.F. Izmaylov, J. Bloino, G. Zheng, J.L. Sonnenberg, M. Hada, M. Ehara, K. Toyota, R. Fukuda, J. Hasegawa, M. Ishida, T. Nakajima, Y. Honda, O. Kitao, H. Nakai, T. Vreven, J.A. Montgomery Jr., J.E. Peralta, F. Ogliaro, M. Bearpark, J.J. Heyd, E. Brothers, K.N. Kudin, V.N. Staroverov, R. Kobayashi, J. Normand, K. Raghavachari, A. Rendell, J.C. Burant, S.S. Iyengar, J. Tomasi, M. Cossi, N. Rega, J. M. Millam, M. Klene, J.E. Knox, J.B. Cross, V. Bakken, C. Adamo, J. Jaramillo, R. Gomperts, R.E. Stratmann, O. Yazyev, A.J. Austin, R. Cammi, C. Pomelli, J.W. Ochterski, R.L. Martin, K. Morokuma, V.G. Zakrzewski, G.A. Voth, P. Salvador, J.J. Dannenberg, S. Dapprich, A.D. Daniels, O. Farkas, J.B. Foresman, J.V. Ortiz, J. Cioslowski, D.J. Fox, Gaussian-09, Revision A.02, Gaussian, Inc., Wallingford CT, 2009.
[25] S.F. Boys, F. Bernardi, Mol. Phys. 19 (1970) 553–566.
[26] N.R. Kestner, J. Chem. Phys. 48 (1968) 252.
[27] H.B. Jansen, P. Ros, Chem. Phys. Lett. 3 (1969) 140.
[28] C. Estarellas, X. Lucas, A. Frontera, D. Quiñonero, P.M. Deyà, Chem. Phys. Lett. 489 (2010) 254.
[29] J.E. Del Bene, J. Phys. Chem. 97 (1993) 107.
[30] J. Alvarez-Idaboy, A. Galano, Theor. Comput. Model. 126 (2010) 75.
[31] S. Salvador, B. Paizs, M. Duran, S. Suhai, J. Comput. Chem. 22 (2001) 765–786.
[32] M.H. Jamroz, Vibrational Energy Distribution Analysis VEDA 4, Warsaw, 2004.
[33] A.P. Scott, L. Random, J. Phys. Chem. 100 (1996) 16502–16504.
[34] G. Keresztury, S. Holly, J. Varga, G. Besenyei, A.Y. Wang, J.R. Durig, Spectrochim. Acta A 49 (1993) 2007–2026.
[35] G. Keresztury, J.M. Chalmers, P.R. Griffith, Raman Spectroscopy: Theory in Handbook of Vibrational Spectroscopy, vol. 1, John Wiley & Sons Ltd., 2002.
[36] Su Qing, Ling Ye, Guang-Di Yang, Ying Mu, Acta Crystallogr. E63 (2007) o1699–o1700.
[37] Y. Wang, S. Saebo, C.U. Pittman Jr., J. Mol. Struct. Theochem. 281 (1993) 91–98.
[38] H.W. Thomson, P. Torkington, J. Chem. Soc. (1945) 640.
[39] E.D. Glendening, J.K. Badenhoop, A.E. Reed, J.E. Carpenter, J.A. Bohmann, C.M. Morales, F. Weinhold, NBO 5.0, Theoretical Chemistry Institute, University of Wisconsin, Madison, 2001.
[40] F. Weinhold, Nature 411 (2001) 539–541.
[41] F. Weinhold, C. Landis, Valency and Bonding: A Natural Bond Orbital Donor–Acceptor Perspective, Cambridge University Press, Cambridge, 2005.
[42] A.E. Reed, L.A. Curtiss, F. Weinhold, Chem. Rev. 88 (1988) 899–926.
[43] M.A. Palafox, J.L. Nunez, M. Gil, J. Mol. Struct. (Theochem.) 593 (2002) 101–106.
[44] I. Lopez Tocon, M.S. Wolley, J.C. Otero, J.I. Marcos, J. Mol. Struct. 470 (1998) 421–425.
[45] D. Sajan, I. Hubert Joe, V.S. Jayakumar, J. Raman Spectrosc. 37 (2005) 508–519.
[46] M. Gussoni, C. Castiglioni, M.N. Ramos, M.C. Rui, G. Zerbi, J. Mol. Struct. 224 (1990) 445–449.
[47] Y. Hung, D.F.R. Gilson, I.S. Butler, J. Chem. Phys. 97 (1993) 1998.
[48] P.S. Kalsi, Spectroscopy of Organic Compounds, sixth ed., New Age International (P) Limited Publishers, New Delhi, 2005.
[49] B.C. Smith, Infrared Spectral Interpretation, A Systematic Approach, CRC Press, Washington, DC, 1999.
[50] N.B. Colthup, L.H. Daly, S.E. Wiberley, Introduction to Infrared and Raman Spectroscopy, Academic Press, New York, 1990.
[51] R.L. Peesole, L.D. Shield, I.C. McWilliam, Modern Methods of Chemical Analysis, Wiley, New York, 1976.
[52] W.O. George, P.S. Mcintyre, Infrared Spectroscopy, John Wiley and Sons, London, 1987.
[53] G. Socrates, Infrared and Raman Characteristic Group Freq, third ed., Wiley, New York, 2001.
[54] E.T.J. Nibbering, T. Elsaesser, Chem. Rev. 104 (2004) 1887.